AIAA JOURNAL
Vol. 49, No. 10, October 2011

Effective Approach for Estimating Turbulence–Chemistry Interaction in Hypersonic Turbulent Boundary Layers

L. Duan* and M. P. Martín†
University of Maryland, College Park, Maryland 20742

DOI: 10.2514/1.J051034

An effective approach for estimating turbulence–chemistry interaction in hypersonic turbulent boundary layers is proposed, based on "laminar-chemistry" Reynolds-averaged Navier–Stokes mean flow solutions. The approach combines an assumed probability density function with a temperature fluctuation scaling, which provides the second moment for specifying the shape of the probability density function. As a result, the effects of temperature fluctuation on chemical production rates can be estimated without solving an additional moment evolution equation. The validity of this method is demonstrated using direct-numerical-simulation data. This approach can be used to identify regions with potentially significant turbulence–chemistry interaction in hypersonic boundary layers, and it provides guidance on whether or not additional efforts need to be taken to model turbulence–chemistry interaction under selected flow conditions.

Nomenclature

c	=	concentration, $c_s = \rho_s/W_s$, mol/m^3
H	=	shape factor, δ^*/θ, dimensionless
h	=	specific enthalpy, J/kg
h°	=	heat of formation, J/kg
K_{eq}	=	equilibrium constant
k	=	reaction rate coefficient or turbulence kinetic energy, $(u'^2 + v'^2 + w'^2)/2$, m^2/s^2
M	=	Mach number, dimensionless
ns	=	total number of species, dimensionless
$Re_{\delta 2}$	=	Reynolds number, $\rho_\delta u_\delta \theta/\mu_w$, dimensionless
Re_θ	=	Reynolds number, $\rho_\delta u_\delta \theta/\mu_\delta$, dimensionless
Re_τ	=	Reynolds number, $\rho_w u_\tau \delta/\mu_w$, dimensionless
T	=	temperature, K
T_a	=	activation temperature, K
u	=	streamwise velocity, m/s
v	=	spanwise velocity, m/s
W	=	molecular weight, kg/mol
w	=	chemical production rate, kg/m^{3}s, or wall-normal velocity, m/s
Y	=	mass fraction, dimensionless
δ	=	boundary-layer thickness, mm
δ^*	=	displacement thickness, mm
θ	=	momentum thickness, mm
ν	=	stoichiometric coefficient, dimensionless
ρ	=	density, kg/m^3

Subscripts

b	=	backward reaction
f	=	forward reaction
s	=	chemical species
w	=	wall variables
x, y, z	=	streamwise, spanwise, and wall-normal directions, respectively, for spatial coordinates
δ	=	boundary-layer edge

Superscript

$+$	=	inner wall units

Received 26 October 2010; revision received 29 March 2011; accepted for publication 5 April 2011.

*Visiting Graduate Student, Department of Aerospace Engineering. Student Member AIAA.

†Associate Professor, Department of Aerospace Engineering. Associate Fellow AIAA.

I. Introduction

THE boundary layers on hypersonic systems, including reentry capsules and airbreathing vehicles, are turbulent and chemically reacting. Fluctuations in temperature and species composition cause fluctuations in species production rate $w_s(T, c_s)$. Because of the nonlinear dependence of w_s on its parameters (primarily temperature), we have

$$\overline{w_s(T, c_s)} \neq w_s(\bar{T}, \bar{c}_s)$$

and the difference is referred to as turbulence–chemistry interaction (TCI), where overbar indicates a mean quantity.

Most previous studies for TCI focused on mixing layers for combustion applications. In turbulent combustion, TCI significantly influences the extent of mixing between high-speed streams of fuel and oxidizer, as well as the reaction rates, and is important for predicting many phenomena such as flame stabilization and ignition time delay [1–7]. Significant efforts have been devoted to model the interrelationship between turbulence and chemistry, and several methods for the closure of the chemical source term have been proposed, one of which is the probability-density-function (PDF) method [6–8].

For hypersonic boundary layers, state-of-the-art calculations have neglected the effects of TCI, and the error introduced by such a simplification is largely uncertain. Duan and Martín [9] investigated TCI in boundary layers under two typical hypersonic conditions, which represent those on blunt and slender-body hypersonic vehicles, respectively, during Earth reentry. They found that TCI has no sizable influence on most mean flow quantities but significantly influences fluctuation quantities, such as temperature and species concentration fluctuations. In addition, they proposed two governing parameters, the interaction Damköhler number and the interaction relative heat release, to measure the mass and heat production effects due to TCI, and demonstrated the effectiveness of these governing parameters in predicting the influence of TCI on flow composition and temperature. However, the evaluation of these governing parameters depends on the knowledge of $\overline{w(T, c)}$, which is not readily available from the mean flow.

Because of the large extent of the parameter space, including permutations of flow conditions, atmospheric and added- or wall-catalytic chemical mechanisms, and the small subset of those that have been explored so far, whether TCI has an effect on the mean flow has not yet been addressed. Because high-order modeling

approaches like direct numerical simulation (DNS) and large-eddy simulation are computationally intensive, and the use of steady-state Reynolds-averaged Navier–Stokes (RANS) models is the tool of choice for routine design purposes [10], it would be useful to have a method to predict the intensity of TCI in the context of RANS before actually doing more expensive simulations, such as DNS, or taking extra efforts to include TCI models.

Martín and Candler [11,12] noticed that for external hypersonic airflows, the chemical source term has a strong temperature dependence. This can be seen by representing the variables as the mean and fluctuating quantities: $T = \bar{T} + T'$ and $c_s = \bar{c}_s + c'_s$. Taking one of the predominant air reactions, binary dissociation of nitrogen $N_2 + M \rightarrow 2N + M$, the source term to a first-order approximation in fluctuating quantities is

$$w_{N_2} = \bar{w}_{N_2} + \bar{w}_{N_2}\left(\left(\frac{T_a}{\bar{T}} + b\right)\frac{T'}{\bar{T}} + \frac{c'_{N_2}}{c_{N_2}} + \frac{c'_M}{\bar{c}_M}\right) + \dots \quad (1)$$

where b is the constant in Eq. (4) and $\bar{w} = w(\bar{T}, \bar{c})$. The variations of w_{N_2} caused by temperature fluctuations may be especially large, because T_a is an order of magnitude larger than typical flow temperatures.

The current study introduces a method to estimate the effects of temperature fluctuations on chemical production rates, or temperature TCI, in the context of RANS. The method combines an assumed PDF [2,6,13,14] with a temperature fluctuation scaling. The assumed PDFs are Gaussian or β distributions, which require values for the first and second moments. The first moment is available from solving the RANS equations, and a temperature scaling (TS) is derived to relate the second moment to the first. In the rest of the paper, this approach is named PDF–TS, i.e., PDF with TS, for simplicity.

The paper is structured as follows. The production rate calculation for finite rate chemistry in chemically reacting flow is given in Sec. II. The definitions of TCI governing parameters and their physical significance are given in Sec. III. The details of PDF–TS method, including the assumed PDF and TS, are introduced in Sec. IV. The DNS validation of PDF–TS is given in Sec. V. Summaries and comments are given in Sec. VI. Finally, conclusions are drawn in Sec. VII.

II. Chemical Production Term

For a reaction

$$\sum_{i=1}^{ns} \nu'_i M_i \rightleftharpoons \sum_{i=1}^{ns} \nu''_i M_i \quad (2)$$

the chemical production rate w_s can be defined by the law of mass action to be

$$\begin{aligned} w_s &= W_s(\nu''_s - \nu'_s)(\omega_f - \omega_b) \\ &= W_s(\nu''_s - \nu'_s)\left(k_f \prod_{i=1}^{ns} c_i^{\nu'_i} - k_b \prod_{i=1}^{ns} c_i^{\nu''_i}\right) \end{aligned} \quad (3)$$

where ν'_i and ν''_i are the stoichiometric coefficients of the reactants and products, respectively. ω_f and ω_b are independent of particular species and can be taken as the reaction rates of the forward and backward reactions, respectively. The forward reaction rate coefficient k_f can be determined from the Arrhenius expression:

$$k_f = AT^b \exp\left(-\frac{T_a}{T}\right) \quad (4)$$

where A and b are constants. The backward reaction rate coefficient is given by

$$k_b = \frac{k_f}{K_{eq}} \quad (5)$$

where the equilibrium constant K_{eq} is a function of T and can be determined using curve fits [15]:

$$K_{eq} = C\exp(A_1/Z + A_2 + A_3 ln(Z) + A_4 Z + A_5 Z^2) \quad (6)$$

where $Z = 10,000/T$, A_1–A_5 are curve-fit coefficients, and C is the unit conversion factor.

Equations (3–5) show that $w_s(T, c)$ depends nonlinearly on its parameters (primarily temperature). As a result, $\overline{w_s(T, c)}$ is usually different from $w_s(\bar{T}, \bar{c})$. The former can be referred as the "turbulent" reaction rate, in which turbulence fluctuations, including both temperature and species fluctuations, have been taken into account, and the latter can be referred as "laminar" reaction rate (although $\bar{T}$ and $\bar{c}_i$ are mean turbulent profiles), which we would obtain if there were no turbulent fluctuations. The greater the difference between the two, the more significant TCI is.

III. Governing Parameters for Estimating Turbulence–Chemistry Interaction

In the study of TCI for hypersonic turbulent boundary layers, Duan and Martín [9] introduced species "interaction" Damköhler number Da_s^I and interaction relative heat release $\overline{\Delta h}^I$ to provide a prediction of the influence of TCI on the turbulent flowfield. The species interaction Damköhler number Da_s^I and interaction relative heat release $\overline{\Delta h}^I$ are defined as

$$\begin{aligned} \mathrm{Da}_s^I &\equiv \left|\frac{(\overline{w_s(T, c)} - w_s(\bar{T}, \bar{c}))\tau_t}{\bar{\rho}_s}\right| \\ \overline{\Delta h}^I &\equiv \frac{\sum_{i=1}^{ns}(\overline{w_i(T, c)} - w_i(\bar{T}, \bar{c}))h_i^\circ \tau_t}{\sum_{i=1}^{ns} \bar{\rho}_i(h_i(\bar{T}) + \frac{1}{2}\tilde{u}_k\tilde{u}_k)} \end{aligned} \quad (7)$$

where τ_t is some turbulence time scale, here defined as the large-eddy turnover time δ/u_δ.

The species interaction Damköhler number represents the relative increase in the species production during the characteristic flow time and is a measure of species production effects due to TCI. The interaction relative heat release represents the relative enhancement in chemical heat release during the characteristic flow time and is a measure of heat production effects due to TCI. If the magnitude of Da_s^I is close to or larger than unity, a significant change in c_s by TCI is expected. When $\overline{\Delta h}^I$ is large, we expect a large influence of TCI on the temperature field. The effectiveness of both parameters for estimating the relative importance of TCI on the flowfield has been demonstrated by Duan and Martín [9].

To investigate the relative importance of temperature TCI alone, on chemical mass and heat production, Da_s^I and $\overline{\Delta h}^I$ are defined as

$$\begin{aligned} \mathrm{Da}_s^I &\equiv \left|\frac{(\overline{w_s(T, \bar{c})} - w_s(\bar{T}, \bar{c}))\tau_t}{\bar{\rho}_s}\right| \\ \overline{\Delta h}^I &\equiv \frac{\sum_{i=1}^{ns}(\overline{w_i(T, \bar{c})} - w_i(\bar{T}, \bar{c}))h_i^\circ \tau_t}{\sum_{i=1}^{ns} \bar{\rho}_i(h_i(\bar{T}) + \frac{1}{2}\tilde{u}_k\tilde{u}_k)} \end{aligned} \quad (8)$$

where $\overline{w_s(T, c)}$ in Eq. (7) has been substituted by $\overline{w_s(T, \bar{c})}$. In the next section, we introduce the PDF–TS method to provide an estimate of $\overline{w_s(T, \bar{c})}$ in the context of RANS simulation.

IV. Probability-Density-Function–Temperature-Scaling Method

In this section, we introduce the PDF–TS method for estimating temperature TCI in the context of RANS by combining an assumed PDF with a temperature fluctuation scaling.

Table 1 Freestream and wall parameters for the larger domain finite volume RANS calculations

M_∞	ρ_∞, kg/m^3	T_∞, K	T_w, K	$h_{t,\infty}$, MJ/kg	α, °
21	0.0184	226.5	2400.0	20	8
21	0.0184	226.5	2400.0	20	35

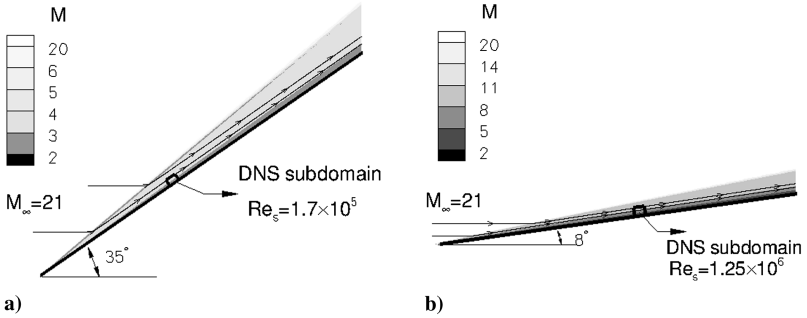

Fig. 1 DNS subdomain from RANS solution for the study of TCI. The Reynolds number $Re_s = \rho_\infty u_\infty s/\mu_\infty$, where s is the distance between the leading edge of the lifting body and the location of the DNS subdomain.

A. Assumed Probability-Density-Function Forms and Parameters

The influence of temperature fluctuation on $\overline{w_s(T,c)}$ manifests itself in $\overline{k(T)}$, where k can be either k_f or k_b, and $\overline{k(T)} \neq k(\bar{T})$. The reaction rate coefficients $\overline{k(T)}$ can be evaluated by the assumed PDF approach, i.e.,

$$\overline{k(T)} = \int_0^\infty k(T)P(T)\,\mathrm{d}T \tag{9}$$

where $P(T)$ is the PDF of T. Several forms of $P(T)$ have been proposed by multiple researchers [2,6,13,14], including the Gaussian PDF and the β PDF. The Gaussian PDF is given by

$$P(T) = \frac{1}{\sqrt{2\pi T'^2_{\mathrm{rms}}}}\exp\left[-\frac{(T-\bar{T})^2}{2T'^2_{\mathrm{rms}}}\right] \tag{10}$$

Thus, the Gaussian PDF is completely determined by $\bar{T}$ and T'^2_{rms}, or $\bar{T}$ and temperature intensity $\frac{T'_{\mathrm{rms}}}{\bar{T}}$.

The β PDF is given by

$$P(r) = \frac{r^{\beta_1-1}(1-r)^{\beta_2-1}}{\Gamma(\beta_1)\Gamma(\beta_2)}\Gamma(\beta_1+\beta_2) \tag{11}$$

where Γ is the gamma function and

$$\beta_1 = \bar{r}\left[\frac{\bar{r}(1-\bar{r})}{\overline{r'r'}} - 1\right]$$

$$\beta_2 = (1-\bar{r})\left[\frac{\bar{r}(1-\bar{r})}{\overline{r'r'}} - 1\right]$$

with $0 < r < 1$. The r in Eq. (11) is related to temperature by the following transformation:

$$r = \frac{T - T_{\min}}{T_{\max} - T_{\min}} \tag{12}$$

The transformation gives

$$\bar{r} = \frac{\bar{T} - T_{\min}}{T_{\max} - T_{\min}} \tag{13}$$

and

$$\overline{r'r'} = \frac{T'^2_{\mathrm{rms}}}{(T_{\max} - T_{\min})^2} \tag{14}$$

Thus, the β PDF is completely determined from $\bar{T}$, T'^2_{rms}, $T_{\min}$, and $T_{\max}$.

The Gaussian PDF and β PDF are completely specified by the mean temperature and temperature fluctuation variance.

B. Temperature Fluctuation Scaling in Hypersonic Boundary Layers

Both the mean temperature and temperature fluctuation variance are needed to specify the assumed Gaussian or β PDFs, as shown in Sec. IV.A. The mean temperature is readily available from the solutions of RANS equations. An additional temperature fluctuation scaling is introduced to connect temperature fluctuation intensity with the flow quantities that can be evaluated using RANS solutions.

Here, we use a generalized version of Huang et al.'s strong Reynolds analogy [16] (HSRA) to relate the temperature fluctuation intensity to the streamwise velocity fluctuation intensity. HSRA has been validated and widely used for nonreacting hypersonic boundary layers with adiabatic and nonadiabatic walls [17–20]. By removing calorically perfect gas assumption used in the derivation, HSRA can be generalized for flows with variable heat capacities and chemical reactions [21]. A cursory description of the derivation of the generalized HSRA is given next.

First, the temperature fluctuations and velocity fluctuations are related using the "mixing length" relation [16,22]:

$$l_u \propto u'_{\mathrm{rms}}/|\partial\bar{u}/\partial z|, \qquad l_T \propto T'_{\mathrm{rms}}/|\partial\bar{T}/\partial z| \tag{15}$$

Table 3 Arrhenius parameters for Eq. (4) for the five-species, five-reaction mechanism (formula 20). The corresponding equilibrium constants are computed from the Gibbs free energy as functions of temperature and then fitted to Park expressions [15]

Reaction	A, m^3/kg s	b	T_a, K
R_1	$7.00e+18$	$-1.60e+00$	113,200
R_2	$2.00e+13$	$-3.82e+00$	59,500
R_3	$5.00e+12$	$+0.00e+00$	75,500
R_4	$6.40e+14$	$-1.00e+00$	38,400
R_5	$8.40e+09$	$+0.00e+00$	19,450

Table 2 Dimensional boundary-layer-edge and wall parameters for the DNS cases. $T_{aw} = T_\infty(1 + r((\gamma-1)/2)M_\infty^2)$ with $r = 0.9$

Cases	M_δ	ρ_δ, kg/m^3	T_δ, K	T_w, K	T_w/T_{aw}	Re_θ	Re_τ	$Re_{\delta 2}$	θ, mm	H	δ, mm
Wedge35supercata	3.4	0.173	4474.5	2400.0	0.13	966.2	906.4	1544.5	0.154	1.79	1.397
Wedge35noncata	3.4	0.172	4505.9	2400.0	0.13	1011.1	910.3	1553.9	0.162	2.18	1.611
Wedge8supercata	9.4	0.070	1290.9	2400.0	0.13	3026.1	786.0	1952.0	0.363	15.0	9.09
Wedge8noncata	9.3	0.072	1234.5	2400.0	0.13	3058.1	741.0	1941.0	0.360	14.9	8.87

Table 4 Curve-fit coefficients for equilibrium constants K_{eq} [Eq. (6)] using Park expressions [15]

Reaction	C	A_1	A_2	A_3	A_4	A_5
R_1	1.e6	$1.6060e+0$	$-1.5732e+0$	$1.3923e+0$	$-1.1553e+1$	$-4.5430e-3$
R_2	1.e6	$6.4183e-1$	$2.4253e+0$	$1.9026e+0$	$-6.6277e+0$	$3.5151e-2$
R_3	1.e6	$6.3817e-1$	$6.8189e-1$	$6.6336e-1$	$-7.5773e+0$	$-1.1025e-2$
R_4	1.0	$9.6794e-1$	$8.9131e-1$	$7.2910e-1$	$-3.9555e+0$	$6.4880e-3$
R_5	1.0	$-3.7320e-3$	$-1.7434e+0$	$-1.2394e+0$	$-9.4952e-1$	$-1.46341e-1$

where l_u and l_T are turbulent mixing length for velocity and temperature, respectively. With $l_u/l_T = Pr_t$ [16], we have

$$T'_{\text{rms}} = f(u'_{\text{rms}}) = \left|\frac{1}{Pr_t}\frac{\partial \bar{T}}{\partial \bar{u}}\right| u'_{\text{rms}} \tag{16}$$

Because for most cases it is the turbulent kinetic energy k rather than the streamwise turbulence intensity u'_{rms} that is readily available in the context of RANS calculations [23], we further relate the streamwise turbulence intensity u'_{rms} in Eq. (16) to the turbulent kinetic energy k by

$$u'_{\text{rms}} = C_M\sqrt{k} \tag{17}$$

where C_M is the proportionality factor. The value of C_M is related to the anisotropy ratios v'_{rms}/u'_{rms} and w'_{rms}/u'_{rms}, which have been found to be insensitive to freestream Mach number, wall temperature, and enthalpy conditions [19–21].

After combining Eqs. (16) and (17), we get a scaling for the temperature fluctuation intensity as

$$T'_{\text{rms}} = C_M\left|\frac{1}{Pr_t}\frac{\partial \bar{T}}{\partial \bar{u}}\right|\sqrt{k} \tag{18}$$

Equation (18) can be used to evaluate T'_{rms} in the context of typical RANS solutions. The right-hand side of Eq. (18) includes mean quantities as well as the turbulent kinetic energy k and turbulent Prandtl number Pr_t, all of which are available in the context of typical RANS calculations, such as standard $k-\varepsilon$ model with the gradient transport model [10,23].

C. Combining Probability Density Function with Temperature Scaling

The steps for using PDF–TS are summarized as follows:

1) Evaluate T'_{rms} using the TS [Eq. (18)].

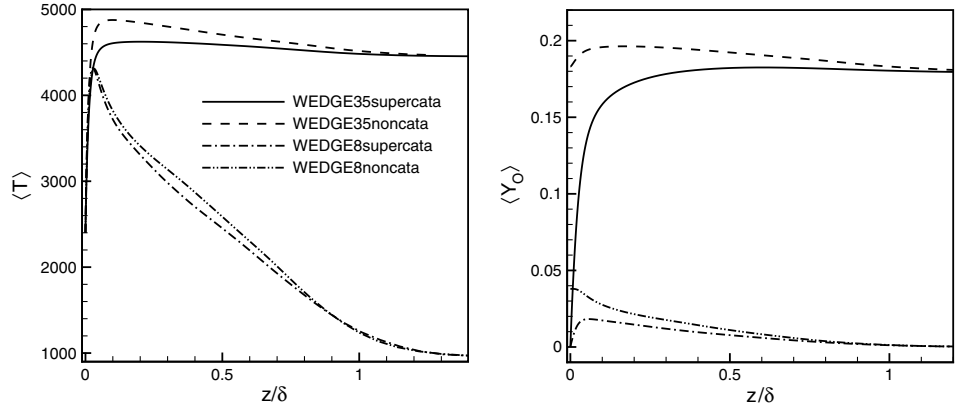

a) b)

Fig. 2 Mean profiles for a) temperature and b) *O* mass fraction.

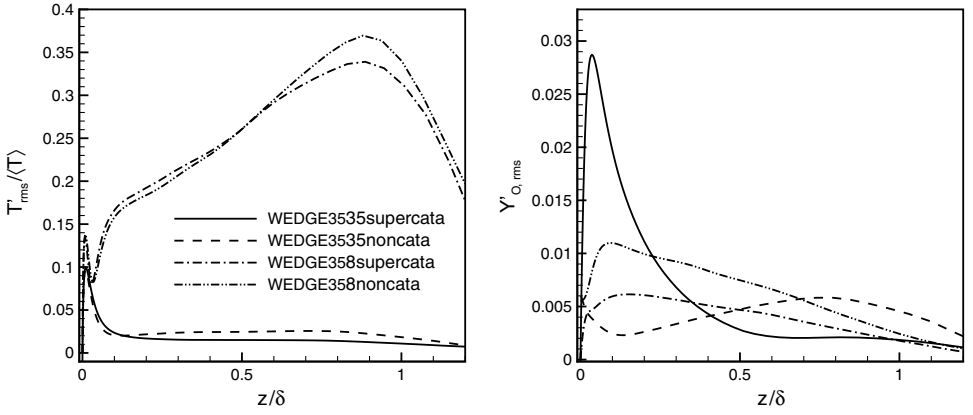

a) b)

Fig. 3 RMS of fluctuations in a) temperature and b) *O* mass fractions.

2) Calculate reaction rate coefficients $\overline{k(T)}$ for each reactions using Eq. (9), with $P(T)$ being Gaussian or β distribution function.

3) Estimate turbulent species production rates $\overline{w_s(T,\bar{c})}$ using the formula

$$\overline{w_s(T,\bar{c})} = W_s(\nu_s'' - \nu_s')\left(\overline{k_f(T)}\prod_{i=1}^{ns}\bar{c}_i^{\nu_i'} - \overline{k_b(T)}\prod_{i=1}^{ns}\bar{c}_i^{\nu_i''}\right) \quad (19)$$

4) Compute temperature TCI intensity $\overline{w(T,\bar{c})} - w(\bar{T},\bar{c})$ as well as the governing parameters Da_s^I and $\overline{\Delta h}^I$, using Eq. (8).

V. Probability-Density-Function–Temperature-Scaling Validation

A. Direct Numerical Simulation of Hypersonic Turbulent Boundary Layers

In this section, we introduce the DNS data that are used to provide a validation for the key assumptions made in deriving PDF–TS as well as the overall performance of PDF–TS. The DNS of hypersonic boundary layers are conducted under typical hypersonic conditions, which represent the boundary layer on a lifting body consisting of a flat plate, flying at 30 km with a Mach number 21 and inclined angles 35 and 8°, denoted as wedge35 and wedge8, respectively. The freestream conditions upstream of the leading-edge shock as well as the wall temperature are given in Table 1. For case wedge35, the large angle of attack results in high postshock temperature and chemically dissociated gas in the boundary-layer edge, and the boundary layer is representative of that on a blunt body. For case wedge8, the angle of attack is small, and the flow at the boundary-layer edge remains cold and nonreacting, although due to recovery effects the temperature rises within the boundary layer and the flow is partially dissociated. The boundary layer in this case is typical of those on a slender-body hypersonic vehicle. For both cases, the boundary-layer-edge conditions for the DNS domain are established by extracting them from a larger domain finite volume RANS calculation using the data parallel line relaxation code [24], which is obtained using a five-species-air-reaction mechanism [Eq. (20)] and considers chemical processes of five species: N_2, O_2, NO, N, and O. Figure 1 sketches the entire computational domain for RANS calculation and the DNS subdomain identified to explore TCI for both conditions. The location of the DNS subdomain is significantly downstream of the leading edge, where the Reynolds number is large enough for the flow to be fully turbulent. In addition, in order to investigate the influence of species boundary conditions on TCI, we consider both "supercatalytic" and "noncatalytic" surface-catalytic models for each flow conditions. The supercatalytic and noncatalytic surface-catalytic models used in the current analysis are representative of the extreme conditions that might happen at the surface of a reentry flight. For simplicity, we refer to wedge35 with supercatalytic wall as wedge35supercata and wedge35 with noncatalytic wall as wedge35noncata. Similar definitions are used for case wedge8. Table 2 lists the boundary-layer-edge conditions and wall parameters for all DNS cases.

The details of DNS, including flow initialization, governing equations and constitutive relations, numerical methods, and data validation are discussed in Duan and Martín [9,21].

The gas-phase reactions in DNS are modeled using the five-species-air-reaction mechanism (N_2, O_2, NO, N, and O) with Arrhenius parameters [15], shown as follows:

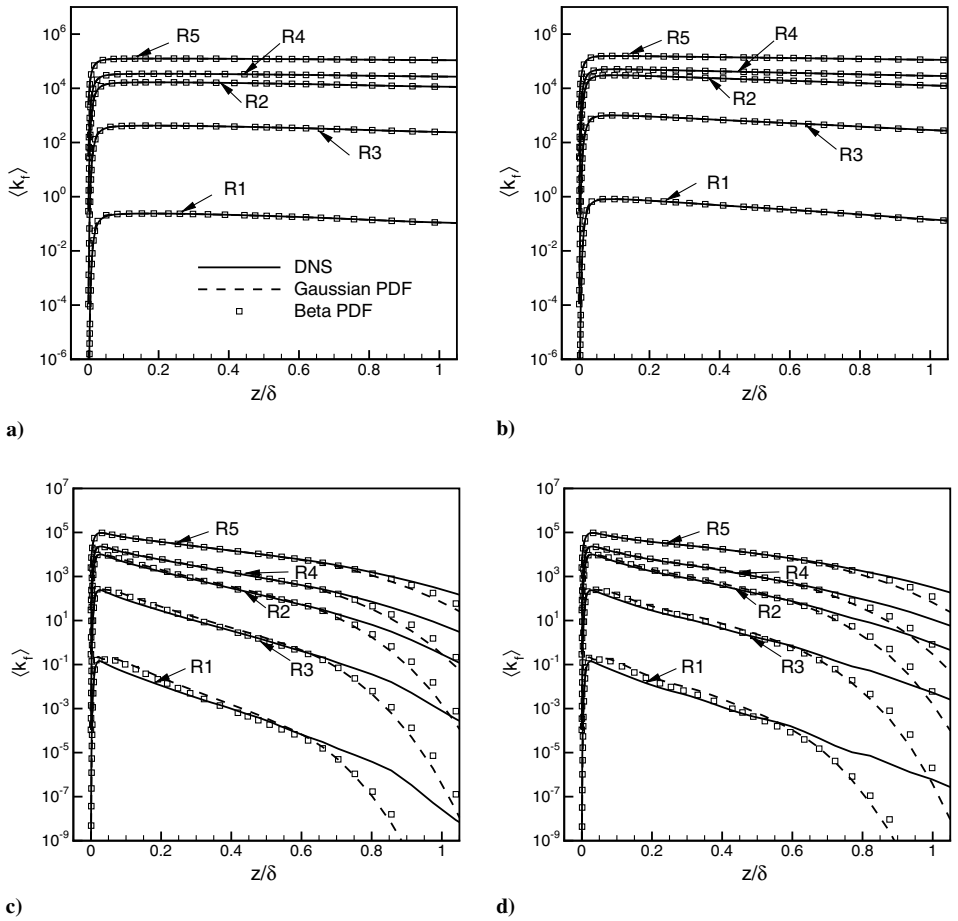

Fig. 4 Mean forward reaction rate constants computed by averaging DNS flowfields and assumed PDF methods: a) wedge35supercata, b) wedge35noncata, c) wedge8supercata, and d) wedge8noncata.

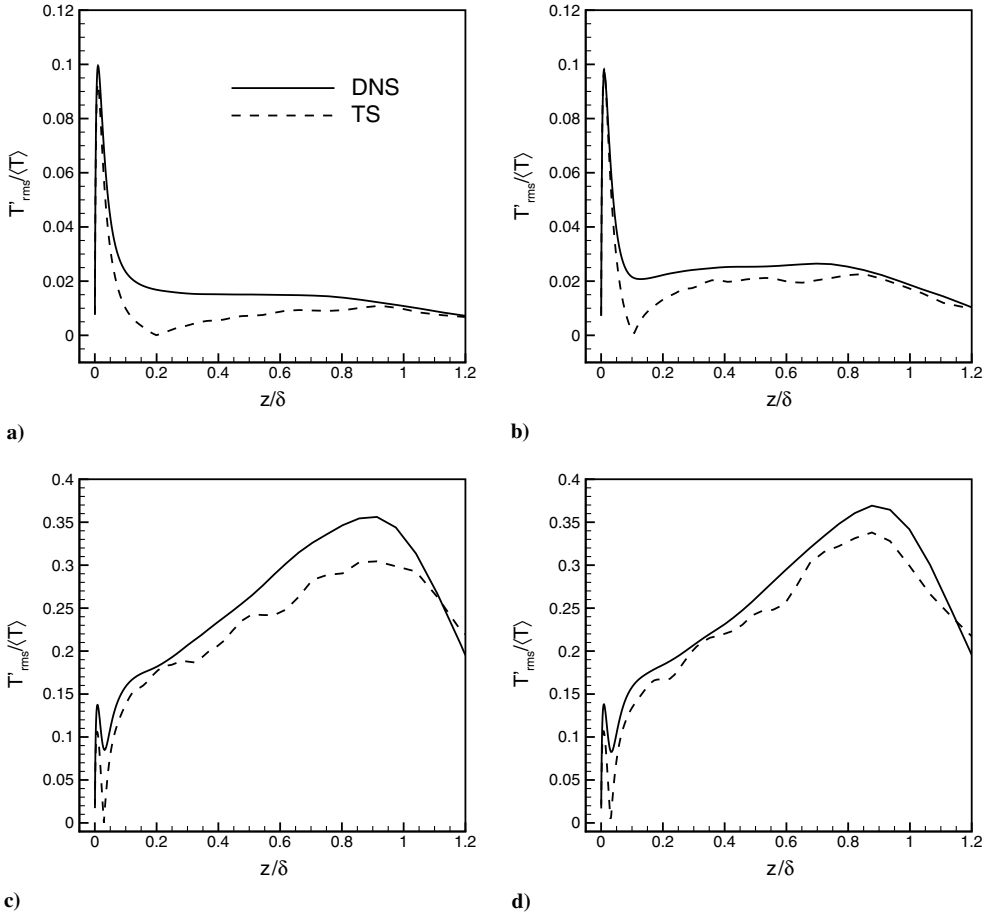

Fig. 5 Temperature fluctuation intensity computed using DNS flowfields or the temperature fluctuation scaling given by Eq. (16). Constant Pr_t is assumed with value 1.0 in the temperature fluctuation scaling: a) wedge35supercata, b) wedge35noncata, c) wedge8supercata, and d) wedge8noncata.

$$\mathrm{N_2} + M \rightleftharpoons 2\mathrm{N} + M \quad (R_1) \qquad \mathrm{O_2} + M \rightleftharpoons 2\mathrm{O} + M \quad (R_2)$$
$$\mathrm{NO} + M \rightleftharpoons \mathrm{N} + \mathrm{O} + M \quad (R_3) \qquad \mathrm{N_2} + \mathrm{O} \rightleftharpoons \mathrm{NO} + \mathrm{N} \quad (R_4)$$
$$\mathrm{NO} + \mathrm{O} \rightleftharpoons \mathrm{O_2} + \mathrm{N} \quad (R_5) \tag{20}$$

with the Arrhenius coefficients in Eq. (4) and the curve-fit coefficients in Eq. (6) given in Tables 3 and 4, respectively. The reacting mechanism represents the realistic reactions of air before ionization happens, which is a good approximation at temperatures less than about 10,000 K.

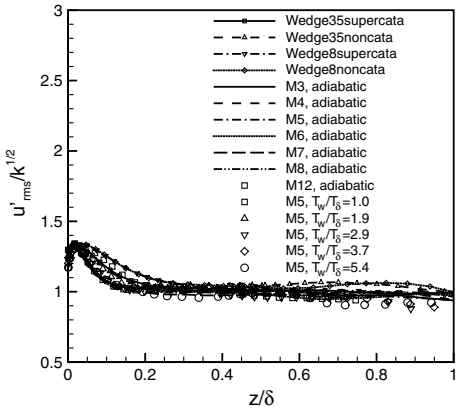

Fig. 6 $\frac{u'_{\mathrm{rms}}}{k^{1/2}}$ computed using DNS flowfields with varying freestream Mach number, wall temperature, and enthalpy conditions [19,20].

At the selected flow conditions, the temperature is high enough to partially dissociate the flow, as shown in Figs. 2a and 2b, in which the mean temperature and the mass fractions of atomic oxygen are plotted. In addition, Figs. 3a and 3b show the levels of fluctuation magnitude in both temperature and species compositions for all cases.

B. Temperature-Scaling Evaluation and Comparison with Direct-Numerical-Simulation Data

To demonstrate the performance of various assumed forms of temperature PDFs, Fig. 4 plots $\overline{k(T)}$, calculated by averaging DNS flowfields or following Eq. (9) using Gaussian or β PDF, for reactions $R1$ to $R5$. The integrations in Eq. (9) for both forms of PDF are numerically performed between $T_{\min} = \bar{T} - 3T'_{\mathrm{rms}}$ and $T_{\max} = \bar{T} + 3T'_{\mathrm{rms}}$ [14]. The results are insensitive to the shape of the PDF for all the cases, similar to the observations by Baurle [25] and Bray and Moss [26] for combustion flows. The match between PDF and DNS results is excellent throughout the boundary layer for wedge35 cases. For case wedge8, good agreement is achieved for $\frac{z}{\delta} \leq 0.6$. At $\frac{z}{\delta} > 0.6$, where $\bar{T}$ is relatively small and there is nearly no chemical reactions, the PDF results underpredict the correct results.

In terms of the performance of the TS, Fig. 5 plots $T'_{\mathrm{rms}}/\overline{T}$, calculated by averaging DNS flowfields or following Eq. (16), for all DNS cases. It is shown that reasonable match between the two is achieved through most of the boundary layer. In particular, the temperature fluctuation scaling correctly predicts the peak location and the general shape of temperature fluctuation intensity. The poor performance of Eq. (16) near the peak location of $\bar{T}$, or the crossover location, where $\partial\bar{T}/\partial z = 0$, can be understood by the fact that the mixing length assumption, where $l_T = T'_{\mathrm{rms}}/(\partial\bar{T}/\partial z)$, no longer holds at $\frac{\partial\bar{T}}{\partial z} \approx 0$.

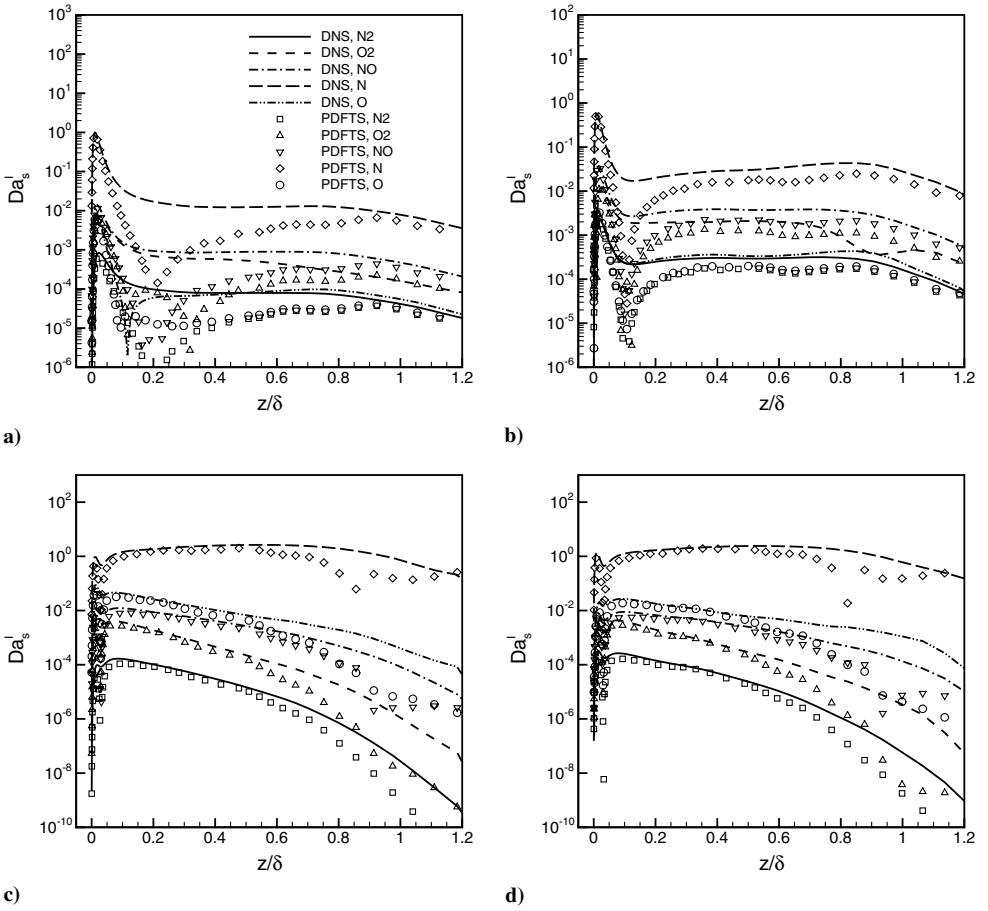

Fig. 7 Interaction Damköhler number Da_s^I computed by averaging DNS flowfields and PDF–TS method. The PDF–TS method combines the Gaussian PDF given by Eq. (10) and the TS given by Eq. (18) with $Pr_t = 1.0$ and the value C_M given by Eq. (21): a) wedge35supercata, b) wedge35noncata, c) wedge8supercata, and d) wedge8noncata.

The insensitivity of the proportionality factor C_M [defined in Eq. (17)] with flow conditions can be demonstrated by DNS results across a wide range of freestream Mach number, wall temperature, and enthalpy conditions, as is shown in Fig. 6. Through most of the boundary layer, C_M can be well approximated as

$$C_M = \frac{\sqrt{2}}{\sqrt{1 + C(1 - e^{-D(z/\delta)})^2}} \tag{21}$$

with $C = 1.06$ and $D = 15$.

To demonstrate the overall performance of PDF–TS, Figs. 7 and 8 plot interaction Damköhler number Da_s^I and relative heat release $\overline{\Delta h}^I$, respectively, computed by averaging DNS flowfields and PDF–TS method for various DNS cases. The PDF–TS method combines the Gaussian PDF given by Eq. (10) and the TS given by Eq. (18), with $Pr_t = 1.0$ and the value C_M given by Eq. (21). It is shown that overall PDF–TS method predicts the governing parameters to the right order through most of the boundary layer. In particular, it correctly captures the peak locations as well as the peak values for various DNS cases. In addition, the relatively poor performance of PDF–TS is observed near $\partial\bar{T}/\partial z \approx 0$, due to the failure of the TS [Eq. (18)].

The validation of the assumed PDFs, the TS, and PDF–TS has been performed against DNS data in different downstream locations along the wedge, and similar performance has been observed.

VI. Summaries and Comments

PDF–TS is a predictive method to estimate the intensity of TCI in hypersonic boundary layers, based on laminar-chemistry RANS calculations. It gives the sensitivity of chemical production rates to temperature fluctuations, as well as an order-of-magnitude estimate of the relative importance of temperature TCI after being combined with the definitions of the governing parameters Da_s^I and $\overline{\Delta h}^I$, and thus it can provide guidance on whether or not to undertake further efforts to model TCI under selected flow conditions.

It should be noted that, so far, only the temperature fluctuation effects of TCI have been considered in PDF–TS, based on the general consideration that the chemical reactions for hypersonic external flows are overall endothermic and dominated by the dissociation of nitrogen and oxygen molecules. These reactions are characterized by very large activation energy, with T_a typically an order of magnitude larger than the maximum flow temperature. As a result, the reaction rate is extremely sensitive to temperature variations. For situations when the species composition fluctuations are equally or more important, the current method provides only a subset of total regions with significant TCI, and the inclusion of species composition fluctuations may be necessary in order to give a more comprehensive evaluation of TCI.

VII. Conclusions

An effective approach is presented to estimate the intensity of TCI. This approach combines an assumed PDF with a temperature fluctuation scaling, named PDF–TS. The assumed PDF is chosen to be either Gaussian or β, and the temperature fluctuation scaling is derived based on well-established boundary-layer relations.

It is shown that the assumed PDF method reproduces DNS results very well, given the accurate mean temperature and temperature fluctuation variance, which are used to specify the shape of PDF. Both Gaussian and β PDF give results with negligible difference. In terms of temperature fluctuation scaling proposed in this paper, it correctly predicts the peak location, the peak value, and the general

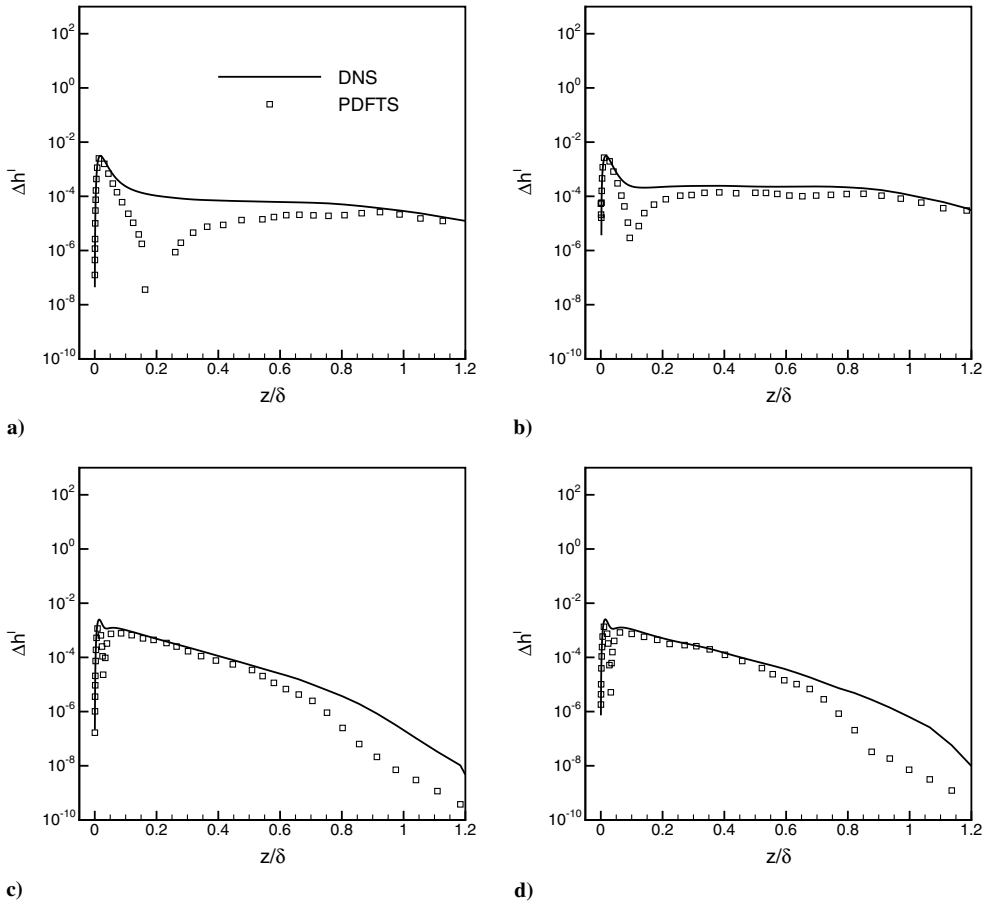

Fig. 8 Interaction relative heat release $\overline{\Delta h'}$ computed by averaging DNS flowfields and PDF–TS method. The PDF–TS method combines the Gaussian PDF given by Eq. (10) and the TS given by Eq. (18) with $Pr_t = 1.0$ and the value C_M given by Eq. (21): a) wedge35supercata, b) wedge35noncata, c) wedge8supercata, and d) wedge8noncata.

shape of temperature fluctuation intensity. It is also shown that the PDF–TS method correctly predicts the chemical production rates as well as nondimensional governing parameters to the right order through most of the boundary layer.

For RANS calculations with TCI neglected, PDF–TS provides a sanity check on whether TCI is negligible. It can also be used to identify regions where TCI could be potentially important, thus providing guidance on whether or not to undertake further efforts to model TCI under selected flow conditions.

Acknowledgment

This work was sponsored by NASA under Grant no. NNX08 AD04A.

References

[1] Libby, P., and Williams, F., *Turbulent Reacting Flows*, Academic Press, New York, 1994.

[2] Gaffney, R.,White, J., Girimaji, S., and Drummond, J., "Modeling Temperature and Species Fluctuations in Turbulent Reacting Flow," *Computing Systems in Engineering*, Vol. 5, No. 2, 1994, pp. 117–133. doi:10.1016/0956-0521(94)90044-2

[3] Delarue, B., and Pope, S., "Calculations of Subsonic and Supersonic Turbulent Reacting Mixing Layers Using Probability Density Function Methods," *Physics of Fluids*, Vol. 10, No. 2, 1998, pp. 487–498. doi:10.1063/1.869536

[4] Hsu, A., Tsai, Y.-L., and Raju, M., "Probability Density Function Approach for Compressible Turbulent Reacting Flows," *AIAA Journal*, Vol. 32, No. 7, 1994, pp. 1407–1415. doi:10.2514/3.12209

[5] Calhoon, W., and Kenzakowski, D., "Assessment of Turbulence–Chemistry Interactions in Missile Exhaust Plume Signature," *Journal of Spacecraft and Rockets*, Vol. 40, No. 5, 2003, pp. 694–695. doi:10.2514/2.6895

[6] Baurle, R., and Girimaji, S., "Assumed PDF Turbulence–Chemistry Closure with Temperature-Composition Correlations," *Combustion and Flame*, Vol. 134, Nos. 1–2, 2003, pp. 131–148. doi:10.1016/S0010-2180(03)00056-7

[7] Gerlinger, P., Noll, B., and Aigner, M., "Assumed PDF Modeling and PDF Structure Investigation Using Finite-Rate Chemistry," *Progress in Computational Fluid Dynamics*, Vol. 5, No. 6, 2005, pp. 334–344. doi:10.1504/PCFD.2005.007066

[8] Pope, S. B., "PDF Methods for Turbulent Reactive Flows," *Progress in Energy and Combustion Science*, Vol. 11, No. 2, 1985, pp. 119–192. doi:10.1016/0360-1285(85)90002-4

[9] Duan, L., and Martín, M. P., "Assessment of Turbulence-Chemistry Interaction in Hypersonic Turbulent Boundary Layers," *AIAA Journal*, Vol. 49, No. 1, 2011, pp. 172–184.

[10] Baurle, R., "Modeling of High Speed Reacting Flows: Established Practices and Future Challenges," AIAA Paper 2004-0267, 2004.

[11] Martín, M., and Candler, G., "Effect of Chemical Reactions on Decaying Isotropic Turbulence," *Physics of Fluids*, Vol. 10, No. 7, 1998, pp. 1715–1724. doi:10.1063/1.869688

[12] Martín, M., and Candler, G., "Subgrid-Scale Model for the Temperature Fluctuations in Reacting Hypersonic Turbulent Flows," *Physics of Fluids*, Vol. 11, No. 9, 1999, pp. 2765–2771. doi:10.1063/1.870135

[13] Frankel, S. H., Drummond, J. P., and Hassan, H. A., "A Hybrid Reynolds Averaged/PDF Closure Model for Supersonic Turbulent Combustion," AIAA Paper 1990-1573, 1990.

[14] Gaffney, R. L., White, J. A., Girimaji, S. S., and Drummond, J. P., "Modeling Turbulent/Chemistry Interactions Using Assumed PDF Methods," AIAA Paper 1992-3638, 1992.

[15] Park, C., *Non-Equilibrium Hypersonic Aerodynamics*, Wiley, New York, 1990.

[16] Huang, P. G., Coleman, G. N., and Bradshaw, P., "Compressible Turbulent Channel Flows: DNS Results and Modelling," *Journal of Fluid Mechanics*, Vol. 305, No. 1, 1995, pp. 185–218.

doi:10.1017/S0022112095004599
[17] Guarini, S. E., Moser, R. D., Shariff, K., and Wray, A., "Direct Numerical Simulation of a Supersonic Turbulent Boundary Layer at Mach 2.5," *Journal of Fluid Mechanics*, Vol. 414, 2000, pp. 1–33. doi:10.1017/S0022112000008466
[18] Maeder, T., Adams, N. A., and Kleiser, L., "Direct Simulation of Turbulent Supersonic Boundary Layers by an Extended Temporal Approach," *Journal of Fluid Mechanics*, Vol. 429, 2001, pp. 187–216. doi:10.1017/S0022112000002718
[19] Duan, L., Beekman, I., and Martín, M. P., "Direct Numerical Simulation of Hypersonic Turbulent Boundary Layers. Part 2: Effect of Wall Temperature," *Journal of Fluid Mechanics*, Vol. 655, 2010, pp. 419–445. doi:10.1017/S0022112010000959
[20] Duan, L., Beekman, I., and Martín, M. P., "Direct Numerical Simulation of Hypersonic Turbulent Boundary Layers. Part 3: Effect of Mach Number," *Journal of Fluid Mechanics*, Vol. 672, 2011, pp. 245–267; also AIAA Paper 2010-0353, 2010.
[21] Duan, L., and Martín, M., "Direct Numerical Simulation of Hypersonic Turbulent Boundary Layers. Part 4: Effects of High Enthalpy," *Journal of Fluid Mechanics*, 2010 (accepted for publication).
[22] Gaviglio, J., "Reynolds Analogies and Experimental Study of Heat Transfer in the Supersonic Boundary Layer," *International Journal of Heat and Mass Transfer*, Vol. 30, No. 5, 1987, pp. 911–926. doi:10.1016/0017-9310(87)90010-X
[23] Wilcox, D. C., *Turbulence Modeling for CFD*, 3rd ed., DCW Industries, La Canada, CA, 2006.
[24] Wright, M. J., T., W., and Mangini, N., "Data Parallel Line Relaxation (DPLR) Code User Manual: Acadia, Version 4.01.1," NASA TM 2009-215388, 2009.
[25] Baurle, R., "Modeling of Turbulent Reacting Flows with Probability Density Function for Scramjet Applications," Ph.D. Dissertation, North Carolina State Univ., Raleigh, NC, 1995.
[26] Bray, K., and Moss, J., "A Unified Statistical Model of Premixed Turbulent Flames," *Acta Astronautica*, Vol. 4, Nos. 3–4, 1977, pp. 291–319. doi:10.1016/0094-5765(77)90053-4

T. Jackson
Associate Editor